MWCNT/V_2O_5 Core/Shell Sponge for High Areal Capacity and Power Density Li-Ion Cathodes

Xinyi Chen,[†] Hongli Zhu,[†] Yu-Chen Chen,[†] Yuanyuan Shang,[‡] Anyuan Cao,[‡] Liangbing Hu,[†,*] and Gary W. Rubloff[†,§,*]

[†]Department of Materials Science and Engineering, University of Maryland, College Park, Maryland 20742, United States, [‡]Department of Materials Science and Engineering, College of Engineering, Peking University, Beijing 100871, People's Republic of China, and [§]Institute for Systems Research, University of Maryland, College Park, Maryland 20742, United States

ABSTRACT

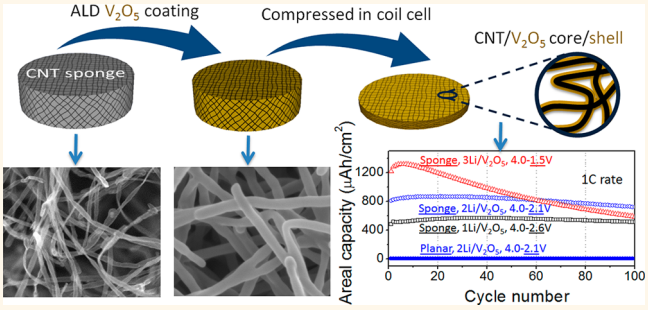

A multiwall carbon nanotube (MWCNT) sponge network, coated by ALD V_2O_5, presents the key characteristics needed to serve as a high-performance cathode in Li-ion batteries, exploiting (1) the highly electron-conductive nature of MWCNT, (2) unprecedented uniformity of ALD thin film coatings, and (3) high surface area and porosity of the MWCNT sponge material for ion transport. The core/shell MWCNT/V_2O_5 sponge delivers a stable high areal capacity of 816 μAh/cm^2 for 2 Li/V_2O_5 (voltage range 4.0−2.1 V) at 1C rate (1.1 mA/cm^2), 450 times that of a planar V_2O_5 thin film cathode. At much higher current (50×), the areal capacity of 155 μAh/cm^2 provides a high power density of 21.7 mW/cm^2. The compressed sponge nanoarchitecture thus demonstrates exceptional robustness and energy-power characteristics for thin film cathode structures for electrochemical energy storage.

KEYWORDS: atomic layer deposition · vanadium oxide · multiwall carbon nanotube · sponge · lithium-ion battery · electrochemical energy storage

Lithium-ion batteries (LIBs) have attracted considerable attention for electrical energy storage with applications in residential energy systems based on renewables, in electric vehicles, and in portable electronic devices and implantable automated systems.[1,2] Next-generation LIBs should provide both high energy and power per unit weight, volume, or area, depending on the applications, to meet requirements for commercialization.[3] With this in mind, significant research efforts have been focused on design and fabrication of nanosized materials and structures because they provide high surface area and short diffusion paths for ionic and electronic conduction, leading to high capacity together with fast kinetics.[4−6] Nanostructures are thus expected to play a significant role in next-generation electrodes, exemplified by a wide variety of studies of silicon nanostructures as anodes.[7−9]

For cathode applications, nanostructured vanadium pentoxide (V_2O_5) has been investigated because it offers several advantages, including high specific capacity (up to 441 mAh/g with three Li de/intercalation per V_2O_5), natural abundance, and better safety than currently used materials.[10−14] Unfortunately V_2O_5 suffers from low electronic conductivity, requiring it to be used in conjunction with another nanostructured material having higher electronic conductivity. For instance, Lee *et al.* deposited V_2O_5 on SnO_2 nanowires for enhanced rate performance.[15] Xue *et al.* reported V_2O_5−SnO_2 double-shelled nanocapsules with high specific capacities.[16]

Carbon nanotubes (CNTs) are particularly attractive in combination with active storage materials because of their excellent electronic conductivity, low density, and good mechanical and chemical stability. A successful strategy reported by several groups is to create interpenetrating networks of CNTs and V_2O_5 nanowires.[17−19] To further reduce electron transport distances, V_2O_5 can be directly deposited on the surface of CNTs; for example, Prakash *et al.* reported commercial CNTs coated and stabilized with 4−5 nm V_2O_5 through a solution-based hydrolysis method.[20] The as-prepared V_2O_5−CNT cathode showed high power density as well as gravimetric and volumetric energy density, but the achievable V_2O_5 mass loading was limited and the cyclability of the material was poor.

* Address correspondence to binghu@umd.edu; rubloff@umd.edu.

Received for review May 31, 2012 and accepted August 7, 2012.

Published online August 07, 2012
10.1021/nn302417x

Inspired by these previous studies, we designed and developed a novel strategy to create high-density assemblies of composite V_2O_5–CNT nanostructures for high-performance cathode applications, featuring a multiwall carbon nanotube (MWCNT) sponge as a structural backbone and nanostructured current collector, and atomic layer deposition (ALD) as a method to deposit V_2O_5 as a coating and to anchor the MWCNTs. The rationale is as follows. The MWCNT sponge has excellent electronic conductivity, high surface area, and high porosity.[21,22] ALD, a powerful technique with unique capabilities such as subnanometer thickness control, extremely high film uniformity, and unparalleled conformality, can exploit this high surface area by conformally coating the CNT sponge.[23−26] The high surface area of the MWCNT and conformal coating capability of ALD enable significantly enhanced loading of active material to achieve high energy density compared to prior work.[20] In addition, the excellent electronic conductivity of MWCNTs in intimate contact with a thin layer of V_2O_5 will profoundly reduce the time required for electron and ion transport during the charge–discharge process, while the high porosity of the MWCNT sponge facilitates ion migration in the electrolyte, all of which are properties essential for high power density.[27,28]

In this paper, we report high areal capacities and rate performance and detailed characterization by electron microscopy and Raman spectroscopy for composite MWCNT/V_2O_5 core/shell nanostructures. The electrochemical performance was studied over different voltage regimes with various charge–discharge rates to explore energy, power, and cycling stability. Electrochemical impedance spectroscopy was also employed to analyze the cycling performance. In summary, our synthesis strategy and nanostructure architecture achieve significantly improved energy and power for high-performance Li-ion cathodes, complementary to previous work on Si–CNT anodes.[22]

RESULTS AND DISCUSSION

Our strategy is shown schematically in Figure 1. We first used chemical vapor deposition (CVD) to grow the MWCNT sponge in a quartz tube at 860 °C, which as-prepared has very low density (~7 mg/cm^3) and high porosity (>99%).[21] Then the sponge was cut into the desired size (typically 0.143–0.174 cm^2, ~2 mm thick) and placed in a commercial ALD reactor, where 1000 cycles of H_2O-based ALD V_2O_5 was deposited on the MWCNT sponge. When the V_2O_5-coated MWCNT sponge was assembled in a coin cell battery, it was compressed from ~2 mm to ~170 μm thickness (see Methods). Since the sponge material is very highly porous, even this 12× compression in one direction will not degrade the ability for ion transport through pores to the active material; that is, the 3D porosity

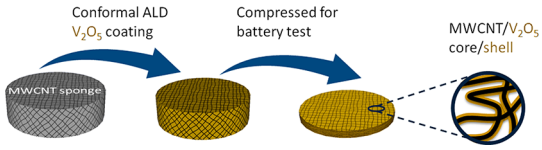

Figure 1. Schematic of experimental flow to fabricate V_2O_5-coated MWCNT sponge. The highly porous MWCNT sponge enables conformal coating of V_2O_5 on the surface of the MWCNT by ALD. The coated MWCNT sponge can be pressed and used as the cathode, where the MWCNT functions as an electron conductor, V_2O_5 functions as Li storage material, and the open pores allow easy electrolyte access. The thickness of the sponge is ~2 mm before and ~170 μm after compression to form a coin cell battery.

is preserved. This is critical for the electrochemical performance especially at high charge–discharge rate, when depletion of ion concentration at the electrolyte/electrode surface could be a limiting factor.[28] A good example can be found in the work by Rinzler *et al.*, where it was shown that engineering the macroporosity of CNT films can double the specific capacitance.[27]

Figure 2 shows scanning electron microscope (SEM) images of the MWCNT sponge before and after ALD V_2O_5 coating, together with a photograph of the sponge (inset of Figure 2a). As expected, the ALD coating is very uniform, and no uncoated MWCNT can be seen after the deposition. The outer diameter of the MWCNT is ~32 nm on average, in line with our previous results.[21] After 1000 cycles of ALD V_2O_5, the outer diameter increased to ~66 nm, indicating a V_2O_5 thickness of ~17 nm. The same ALD process on planar Si substrates gave a larger measured thickness of ~30 nm, suggesting a significant nucleation barrier for the ALD process on the MWCNT surface. This would not be surprising since the surface of the MWCNT is generally free of hydroxyl or carboxyl groups and thus relatively inert to ALD. Previous studies indicated that the nucleation inhibition can be overcome by surface functionalization using HNO_3 acid or NO gas.[29,30] Alternatively, the reduced growth rate could also result if precursor doses were not high enough to saturate the surface reaction over the unusually high surface area of the sponge, as discussed further below. While we are continuing to investigate the surface modification of MWCNTs, ALD recipe optimization, and the novel O_3-based ALD V_2O_5 process we developed recently,[31] the nanocomposite sponge structure displays significant electrochemical performance, which we focus on here.

Transmission electron microscopy (TEM) also shows that uniform V_2O_5 coatings over individual MWCNTs were achieved using H_2O-based ALD (Figure 3a). The desired MWCNT/V_2O_5 coaxial structure can be well resolved in higher magnification TEM images (Figure 3b and c). The energy-dispersive X-ray spectroscopy (EDX) in the inset of Figure 3b shows clear evidence of core/shell tubular structure with the V and O signal peaks at the outside (shell) of the composite

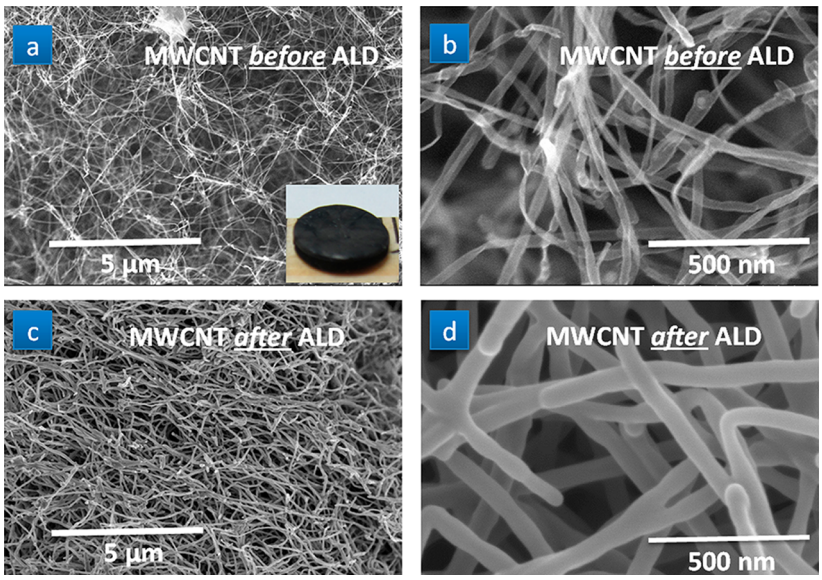

Figure 2. SEM images of MWCNT sponge (a, b) before and (c, d) after 1000 cycles of ALD V_2O_5 coating. Inset of (a) shows an optical photograph of the MWCNT sponge with 6.4 mm diameter × 2 mm thickness.

nanotube and the C signal peak at the inner part (core) of the tube. The interface between V_2O_5 and MWCNT can also be distinguished from the gray scale contrast across the nanotube, according to the TEM-based methodology developed in our laboratory for nanotube analysis.[32] No diffraction features are seen from the V_2O_5 layer, which indicates it is amorphous, consistent with our previous result.[33]

The thickness of the V_2O_5 layer as observed by TEM is only 4−6 nm, less than the ∼17 nm measured in SEM. It can be presumed that the penetration of the ALD film into the sponge may be limited, given the high surface area and aspect ratio, as well as the tortuous structure of the sponge, leading to thinner films in the middle of the sponge than at the surface. Since the SEM observation focuses on the surface of the sponge while the TEM observation originates from a random location in the sponge, limited penetration of the ALD film into the sponge will cause smaller thicknesses observed in TEM than in SEM, as found here. This might be regarded as nonideal conformity, albeit on a considerably larger length scale than the film uniformity over high aspect ratio MWCNTs. Indeed, the thickness depletion from the surface to the inner part is not uncommon for ALD coatings on very high aspect ratio structures.[34]

The MWCNT sponge was also characterized with Raman spectroscopy before and after ALD coating, showing the expected MWCNT and V_2O_5 (see Figure 1S and supplemental discussions). With clear evidence for the successful synthesis of the MWCNT/V_2O_5 core/shell sponge, samples were incorporated into coin cells for electrochemical performance tests. The MWCNT/V_2O_5 sponge cathodes were tested in a half-cell configuration using Li metal as the standard anode. To fully explore the capacities, we chose three voltage ranges, 4.0−2.6, 4.0−2.1, and 4.0−1.5 V, which correspond respectively to one, two, and three lithium intercalations per formula unit V_2O_5 (abbreviated below as 1Li/V_2O_5, 2Li/V_2O_5, 3Li/V_2O_5).[10] While we found that the capacity of the sponge tested at 1C is as high as 82% of that at 1C (see Figure 2Sa), we performed most tests at 1C or higher rates (*n*C means charge/discharge of the battery with 1/*n* hours). Since the sponge was only ∼170 μm thick after compression, an attractive (though not unique) application would be in a microbattery, where the capacity per unit substrate area is of particular interest.[35,36] The charge−discharge curves plotted as voltage *vs* areal capacity at the second cycle are shown in Figure 4a. No plateau can be observed at any voltage range during charge−discharge procedures, indicating the absence of phase transitions typical of the Li (de)/insertion for crystalline V_2O_5 films.[10] The absence of plateaus has been reported before as a characteristic for amorphous films.[37] To exclude the contribution of double-layer capacitance from MWCNT, we tested the sample with MWCNT only and found more than 98% of the stored charge is from V_2O_5 (see Figure 2Sb).

The corresponding capacities for the second discharge cycle for 1Li/V_2O_5, 2Li/V_2O_5, and 3Li/V_2O_5 are 514, 818, and 1284 μAh/cm^2, respectively. These values are all larger than those for commercial planar Li-ion microbatteries (113 μAh/cm^2)[38] and comparable to most state-of-the-art three-dimensional microbatteries (in the range of 1 mAh/cm^2).[5]

The sponge architecture provides a dramatic enhancement of storage capacity. For 2Li/V_2O_5 (4.0−2.1 V), we compared the areal capacity of the MWCNT/V_2O_5 sponge with a thin V_2O_5 film simultaneously deposited on a planar stainless steel disk (Figure 4b). The second cycle discharge capacity for the planar

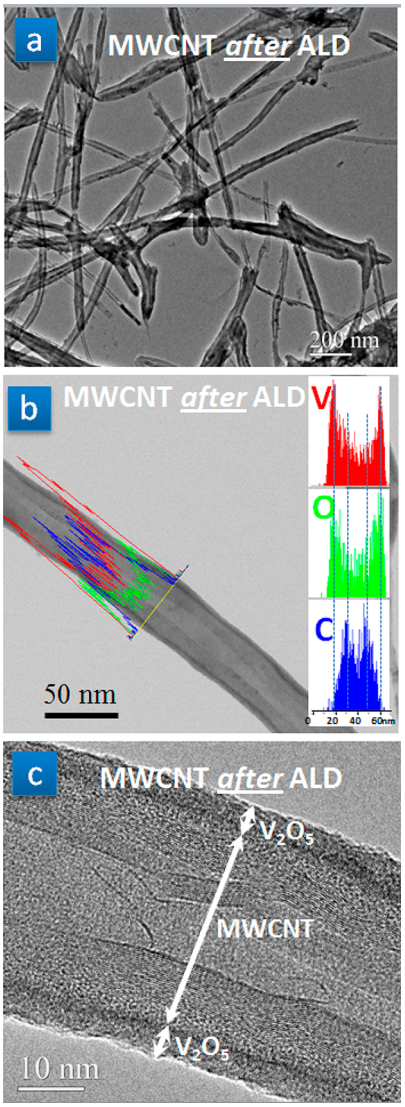

Figure 3. (a) TEM image of MWCNT coated with ALD V_2O_5 showing uniform coating. (b, c) High-magnification TEM images, where the coaxial structures of MWCNT and V_2O_5 are well resolved and distinguished by the EDX line scans across the nanostructure shown in the inset of (b) and by the gray scale contrast in (c).

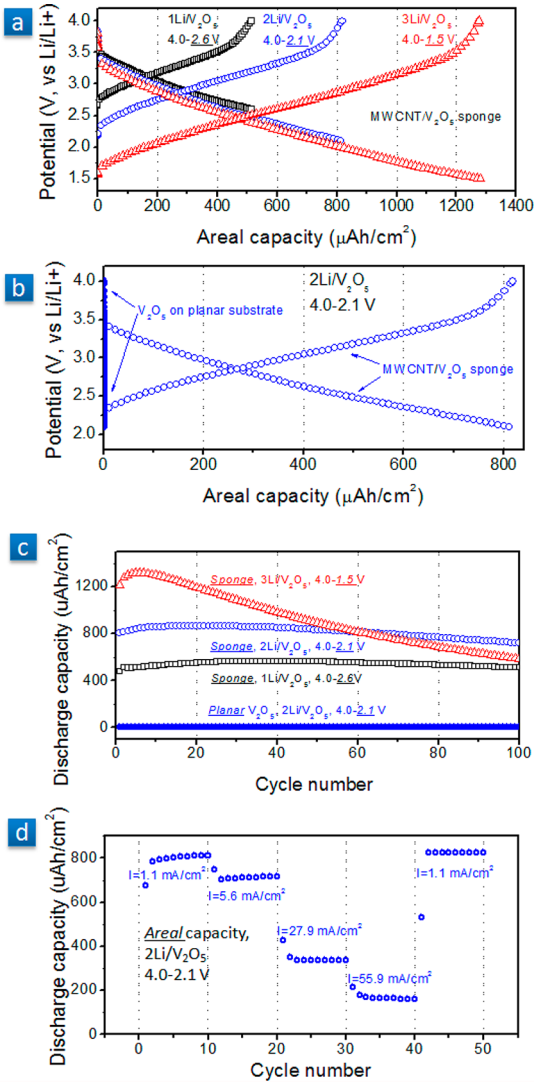

Figure 4. (a) Discharge and charge curves (second cycle) for the cells with MWCNT/V_2O_5 sponge cathodes in three different voltage ranges with 1C current. (b) Discharge and charge curves (second cycle) of the cells with planar and MWCNT/V_2O_5 sponge cathodes in the voltage range for 2Li/V_2O_5 (4.0−2.1 V) with 1C current. (c) Cycling performance and areal capacity comparison between the cell with planar V_2O_5 cathode in the voltage range for 2Li/V_2O_5 (4.0−2.1 V) and the cells with MWCNT/V_2O_5 sponge cathodes in three different voltages with 1C current. (d) Rate capability data for MWCNT/V_2O_5 sponge cathodes in the voltage range for 2Li/V_2O_5 (4.0−2.1 V) at different current densities as indicated.

V_2O_5 film is only 1.8 μAh/cm^2, while the sponge delivered a dramatically higher capacity of −818 μAh/cm^2, a 453× increase. This increase is primarily attributed to the high surface area of the sponge that enabled 517× more V_2O_5 (determined from measured mass), but more importantly to the superior nanoarchitecture that makes most of the V_2O_5 easily accessible for Li (de)/intercalation on a short time scale. We note that this areal capacity enhancement (453×) is significantly higher than other designs using 3D microchannels (20−30×),[36] free-standing Al nanorods (10×),[39] and biotemplated nanowire forest (~8×).[40]

The performance of the cells cycled at various voltage ranges (Figure 4c) shows excellent cycling stability for 1Li/V_2O_5 and 2Li/V_2O_5 (4.0−2.6 and 4.0−2.1 V), with only modest decay after 100 cycles (<0.1% decay per cycle). In contrast, for 3Li/V_2O_5 (4.0−1.5 V), the capacity decay was much larger, *i.e.*, 49% capacity loss after 100 cycles (0.49% decay per cycle). However, this decay was not as fast as that reported for V_2O_5/SnO_2 nanowires, which lost 38% capacity after only 15 cycles at 4.0−1.8 V (2.5% decay per cycle).[15]

There was an obvious increase in capacity for 3Li/V_2O_5 (4.0−1.5 V) at the first five cycles, which is quite different from that in the other two voltage ranges. This "warm-up" behavior is possibly due to the improved

wetting of electrolyte−electrode interphase, especially for nanoscale composite electrode materials.[41] In addition, we propose another possible proton exchange mechanism. The thermogravimetric analysis (TGA) in Figure 3S showed about 3% weight loss between 100 and 325 °C due to residual water-related species in the film. In the first few cycles, the associated protons in the V_2O_5 film could be extracted while Li is extracted during charge, leaving sites open for additional Li insertion during the next discharge. That this behavior is more obvious at 4.0−1.5 V than 4.0−2.1 and 4.0−2.6 V could be explained by the fact that the residual H_2O-related species in V_2O_5 is fairly stable and thus a wider range of voltage is required to make the proton exchange happen.

Figure 4d shows results from rate capability experiments for the MWCNT/V_2O_5 sponge cathodes upon cycling at different current densities of 1.1, 5.6, 27.9, and 55.9 mA/cm^2 (corresponding to 1C, 5C, 25C, and 50C, respectively). At each current, the battery was tested for 10 cycles to ensure the reliability of the reported readings. The specific capacity was stable at a constant current rate, while changes in current density resulted in stepwise dependence of the areal capacity. The sponge cathodes were able to provide 90%, 44%, and 22% of the initial capacity at 1C rate when the cycling current was increased by 5, 25, and 50 times. When tested at 55.9 mA/cm^2, the areal capacity was 155 μAh/cm^2. The calculated energy densities at 1.1 and 55.9 mA/cm^2 are 2.29 and 0.43 mWh/cm^2, corresponding to power densities as high as 2.29 and 21.7 mW/cm^2, respectively.

This rate performance is somewhat better than that previously found for Al nanorods coated with 17 nm ALD TiO_2.[39] There the authors reported 35% capacity retention from C/5 to 20C, while our MWCNT/V_2O_5 sponge showed 44% retention from 1C to 25C. We believe this good rate performance originates from the structure of the MWCNT/V_2O_5 sponge, which provides excellent electronic conduction, short charge carrier (both e^- and Li^+) transport path lengths over the V_2O_5 layer, and easy access of the electrolyte to the increased surface area.

Gravimetric capacity results (see Figure 4S and supplemental discussions) show similar benefits in performance to those presented here for areal capacity behavior. However, the V_2O_5 loading was relatively small (~50% by weight), and future reports will treat gravimetric/volumetric capacity with higher loading.

We found that the Coulombic efficiency (Figure 5a) for 3Li/V_2O_5 (4.0−1.5 V) is consistently lower than that for 2Li/V_2O_5 (4.0−2.1 V), supporting the cycling performance shown in Figure 4c. We performed analysis using electrochemical impedance spectroscopy (EIS) to understand the decay mechanism, with results shown in Figure 5b and c. The spectra were fitted using an equivalent circuit (EC), shown in the inset of

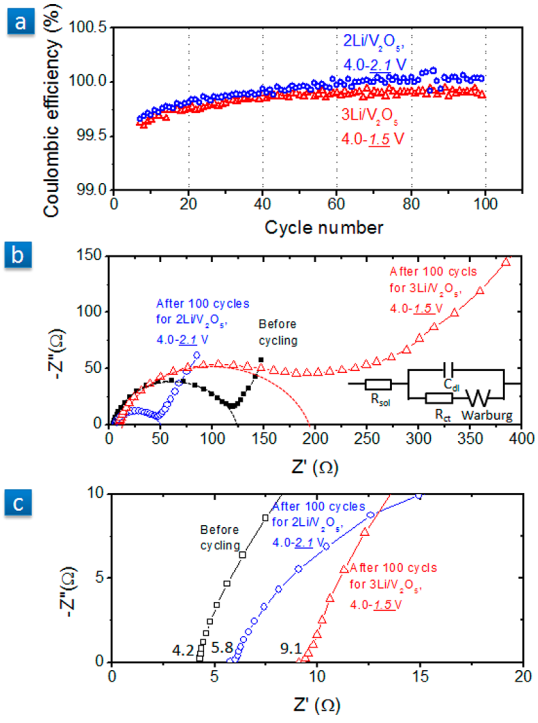

Figure 5. (a) Comparison of Coulombic efficiency for the cells cycled for 2Li/V_2O_5 (4.0−2.1 V) and 3Li/V_2O_5 (4.0−1.5 V). (b, c) EIS data collected from the cells with MWCNT/V_2O_5 sponge cathodes before cycling and after 100 charge−discharge cycles for 2Li/V_2O_5 (4.0−2.1 V) and 3Li/V_2O_5 (4.0−1.5 V). Inset of (b) shows the equivalent circuit of the cell.

Figure 5b. The proposed EC was $R_{sol}(C_{dl}[R_{CT}W])$, where R_{sol} represents the electrolyte resistance, C_{dl} the double-layer capacitance, and R_{CT} the charge-transfer resistance at the V_2O_5−electrolyte interface, which is in serial connection with the Warburg element (W). There are two major changes after 100 cycles for 2Li/V_2O_5 (4.0−2.1 V) and 3Li/V_2O_5 (4.0−1.5 V). First, the enlarged semicircle diameter indicates an increase of resistance for charge transfer at the V_2O_5−electrolyte interface when cycled for 3Li/V_2O_5 (4.0−1.5 V), in contrast with a decrease of charge-transfer resistance when cycled for 2Li/V_2O_5 (4.0−2.1 V). This is possibly associated with a higher resistive solid electrolyte interphase (SEI) formation for 3Li/V_2O_5 (4.0−1.5 V). In contrast, the enhanced wetting between electrolyte and electrode after cycling might be responsible for the decrease in charge-transfer resistance for 2Li/V_2O_5 (4.0−2.1 V), where the SEI formation is not significant because of the higher cutoff voltage. Second, the electrolyte resistance, as indicated by the real part of the impedance at high frequencies, has increased from 4.2 to 9.1 Ω when cycled for 3Li/V_2O_5 (4.0−1.5 V), larger than 5.8 Ω for 2Li/V_2O_5 (4.0−2.1 V). This may result from dissolution of active material into electrolyte 3Li/V_2O_5 (4.0−1.5 V), as indicated by previous studies on V_2O_5-based materials,[15,20] or from consumption of electrolyte during SEI formation.

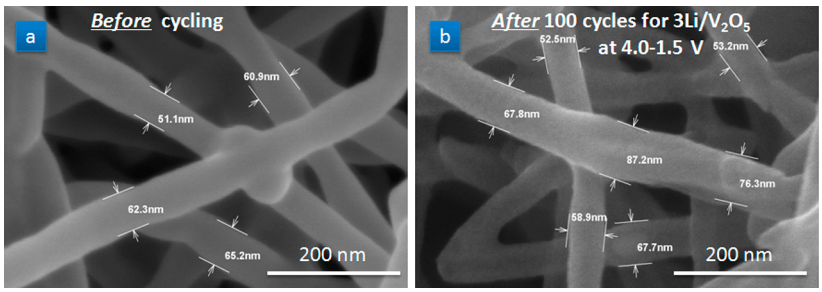

Figure 6. SEM images of MWCNT/V_2O_5 sponge (a) before and (b) after electrochemical testing for 3Li/V_2O_5 (4.0−1.5 V) for 100 cycles, showing the stability of the core/shell structure.

Finally, we looked at the morphology of the sponge after cycling 3Li/V_2O_5 (4.0−1.5 V) and compared it with that of fresh sponge (Figure 6). No obvious change in the morphology can be observed except that the surface became rough after cycling, probably associated with the SEI formation. More importantly, no uncoated MWCNT exists, demonstrating the stability of the coaxial structure of MWCNT/V_2O_5 upon electrochemical cycling. Therefore, we conclude the decay for 3Li/V_2O_5 (4.0−1.5 V) was primarily caused by the intrinsic property of V_2O_5, but no link to structure failures could be found.

CONCLUSIONS

We have successfully fabricated MWCNT/V_2O_5 sponges designed for high electrochemical performance. The high surface area of the sponge allows for a significant amount of active material loading. Electrons can freely transport through the MWCNTs. The thin uniform layer of V_2O_5 (<16 nm) enables (de)/lithiation in active material within a very short time. The high porosity of the sponge provides easy access of electrolyte to the active storage material. The MWCNT/V_2O_5 sponge delivered a high initial areal capacity of 1284 μAh/cm^2 for 3Li transfer (4.0−1.5 V), although cyclability was poor. EIS results showed an increase in charge-transfer resistance after cycling, probably due to the dissolution of V_2O_5 and the formation of a higher resistive SEI layer. SEM confirmed that the MWCNT/V_2O_5 core/shell structure, however, was stable after electrochemical cycling. The cycling stability was largely improved using a larger discharge cutoff voltage. In the 4.0−2.1 V range for 2Li/V_2O_5, the initial areal capacity was 818 μAh/cm^2 at 1C and maintained a capacity of 155 μAh/cm^2 with 50C rate, giving a high power density of 21.7 mW/cm^2. We suggest initial application of such a sponge cathode primarily for thin film batteries, although other applications to larger energy storage challenges may follow. For larger scale LIBs, the ALD recipe for optimization and/or surface functionalization of MWCNTs is required for coating larger scale samples efficiently. Overall, this work demonstrates an effective approach to engineer MWCNTs with a metal oxide coating for high-performance electrochemical energy storage.

METHODS

MWCNT/V_2O_5 Sponge Preparation. Carbon nanotube sponges were synthesized by chemical vapor deposition using 1,2-dicyclobenzene as the carbon source and ferrocene as the catalyst. Ferrocene powder was dissolved into 1,2-dicyclobenzene to make a solution with a concentration of 0.06 g/mL. Then the source solution was injected into a 2 in. quartz tube housed in a CVD furnace by a syringe pump at a constant feeding rate of 0.13 mL/min. The carrying gas is a mixture of Ar and H_2, at a flow rate of 2000 and 300 mL/min, respectively. Quartz slides were used as the growth substrate to deposit nanotubes in the center of the furnace at a set reaction temperature of 860 °C. Typically the growth time was 4 h, which gives bulk sponge samples with thicknesses of about 8−10 mm. The sponge was then cut into the desired size before ALD coating.

The ALD V_2O_5 coating was done using a BENEQ TFS 500 reactor with a 2 mbar base pressure. $VO(OC_3H_7)_3$ was used as the vanadium precursor, which was kept at 45 °C with a vapor pressure of 0.29 Torr. The VTOP pulse is controlled with ALD valves, which first introduce N_2 to the precursor supply vessel through an upstream ALD valve and then deliver the headspace gas through a downstream ALD valve. Deionized water was used as the oxidizing agent in the ALD V_2O_5 process. The temperature for H_2O-based ALD was set at 120 °C. In the same batch for ALD coating on MWCNT, both a Si wafer and a stainless steel disk were put in the reaction chamber. The Si wafer was used for thickness measurement on the planar substrate, which was done by a SOPRA GES5 spectroscopic ellipsometer. The stainless steel disk was used as the substrate and current collector for the planar V_2O_5 film, which was tested later as the cathode to compare with the sponge cathodes. All films were grown with 1000 cycles, each being 2 s VTOP pulse, 2 s N_2 purge, 4 s H_2O pulse, and 4 s N_2 purge.

Structure Characterization and Electrochemical Tests. The morphology of the ALD films was investigated by a Hitachi SU-70 high-resolution scanning electron microscope. After battery testing samples were washed in acetonitrile to remove the electrolyte before being introduced to the SEM. The structural features and composition of the electrode materials were investigated using transmission electron microscopy (JEOL 2100F field emission TEM) with EDX. The TEM sample was prepared by ultrasonicating the MWCNT/V_2O_5 sponge in the acetone solvent. Raman spectroscopy was performed in a Horiba Jobin-Yvon LabRAM HR-VIS MicroRaman system with an internal 632.8 nm laser source.

Electrochemical experiments were carried out in the half-cell configuration in standard coin cells (R032), which were assembled in an argon environment glovebox with an oxygen concentration of less than 0.5 ppm. The MWCNT/V_2O_5 sponge and the planar V_2O_5 on a stainless steel disk served as the cathodes, which were baked in a vacuum oven at 100 °C overnight before cell assembly. Lithium foil (Sigma Aldrich, MO, USA)

served as the anode, and a Celgard separator (Celgard 3501) was placed between the two electrodes and soaked with the electrolyte (1 M $LiPF_6$ solution in ethyl carbonate/diethyl carbonate (1:1), Novolyte Technologies, OH, USA). All the parts were compressed in a crimping machine with 750 psi. The mass of the active material was determined by weight measurements with a high-precision microbalance (Mettler Toledo, XS105 dualRange, 1 μg resolution) before and after V_2O_5 deposition. The typical mass of the V_2O_5 loaded on the MWCNT sponge (0.143−0.174 cm^2, ~2 mm thick) was 0.505−0.713 mg. The mass of deposited V_2O_5 over total MWCNT/V_2O_5 sponge varied from 47% to 60%. After the battery cycling, the cell was taken apart, and the thickness of the sponge measured with a microcalliper was ~170 μm. Galvanostatic experiments were carried out using a multiple-channel battery test station (Arbin Instruments, TX, USA), while EIS data were collected from a Bio-Logic VMP3 using the EC-Lab software.

Conflict of Interest: The authors declare no competing financial interest.

Acknowledgment. This work has been supported by Nanostructures for Electrical Energy Storage (NEES), an Energy Frontier Research Center funded by the U.S. Department of Energy, Office of Science, Office of Basic Energy Sciences, under Award No. DESC0001160, which supported the work of X.C. and G.R. L. H. acknowledges startup support from University of Maryland College Park and affiliation with NEES. The Maryland group (X.C., H.Z., Y.C., L.H., and G.R.) produced the MWCNT/V_2O_5 core/shell sponge and carried out the materials and electrochemical characterization. Y.S. and A.C. prepared the MWCNT sponge. A.C. thanks the Beijing Natural Science Foundation (Program No. 8112017) for financial support. We also acknowledge the support of the Maryland NanoCenter and its NispLab.

Supporting Information Available: Raman spectrum of MWCNT sponge before and after ALD of V_2O_5, gravimetric discharge curves for MWCNT/V_2O_5 sponge at C/20 and 1C rate, discharge curves for V_2O_5-coated MWCNT and MWCNT only, TGA curve for V_2O_5, electrochemical performance of MWCNT/V_2O_5 sponge described with gravimetric data. This material is available free of charge *via* the Internet at http://pubs.acs.org.

REFERENCES AND NOTES

1. Tarascon, J. M.; Armand, M. Issues and Challenges Facing Rechargeable Lithium Batteries. *Nature* **2001**, *414*, 359–367.
2. Scrosati, B.; Garche, J. Lithium Batteries: Status, Prospects and Future. *J. Power Sources* **2010**, *195*, 2419–2430.
3. Kang, B.; Ceder, G. Battery Materials for Ultrafast Charging and Discharging. *Nature* **2009**, *458*, 190–193.
4. Roberts, M.; Johns, P.; Owen, J.; Brandell, D.; Edstrom, K.; Enany, G. E.; Guery, C.; Golodnitsky, D.; Lacey, M.; Lecoeur, C.; *et al.* 3D Lithium Ion Batteries—From Fundamentals to Fabrication. *J. Mater. Chem.* **2011**, *21*, 9876–9890.
5. Oudenhoven, J. F. M.; Baggetto, L.; Notten, P. H. L. All-Solid-State Lithium-Ion Microbatteries: A Review of Various Three-Dimensional Concepts. *Adv. Energy Mater.* **2011**, *1*, 10–33.
6. Centi, G.; Perathoner, S. The Role of Nanostructure in Improving the Performance of Electrodes for Energy Storage and Conversion. *Eur. J. Inorg. Chem.* **2009**, *26*, 3851–3878.
7. Chen, H.; Xu, J.; Chen, P.; Fang, X.; Qiu, J.; Fu, Y.; Zhou, C. Bulk Synthesis of Crystalline and Crystalline Core/Amorphous Shell Sillicon Nanowires and Their Application for Energy Storage. *ACS Nano* **2011**, *5*, 8383–8390.
8. Hwang, T. H.; Lee, Y. M.; Kong, B. S.; Seo, J. S.; Choi, J. W. Electrospun Core-Shell Fibers for Robust Silicon Nanoparticle-based Lithium Ion Battery Anodes. *Nano Lett.* **2012**, *12*, 802–807.
9. Chan, C. K.; Peng, H.; Liu, G.; McIlwrath, K.; Zhang, X. F.; Huggins, R. A.; Cui, Y. High-Performance Lithium Battery Anodes Using Silicon Nanowires. *Nat. Nanotechnol.* **2008**, *3*, 31–35.
10. Whittingham, M. S.; Song, Y.; Lutta, S.; Zavalij, P. Y.; Chernova, N. A. Some Transition Metal (oxy)phosphates and Vanadium Oxides for Lithium Batteries. *J. Mater. Chem.* **2005**, *15*, 3362–3379.
11. Wang, Y.; Cao, G. Developments in Nanostructured Cathode Materials for High-Performance Lithium-Ion Batteries. *Adv. Mater.* **2008**, *20*, 2251–2269.
12. Fang, W.; Fang, W. Fast and Reversible Surface Redox Reduction in V_2O_5 Dispersed on CN_x Nanotubes. *Chem. Commun.* **2008**, *41*, 5236–5238.
13. Chan, C. K.; Peng, H.; Twesten, R. D.; Jarausch, K.; Zhang, X. F.; Cui, Y. Fast, Completely Reversible Li Insertion in Vanadium Pentoxide Nanoribbons. *Nano Lett.* **2007**, *7*, 490–495.
14. Yu, D.; Chen, C.; Xie, S.; Liu, Y.; Park, K.; Zhou, X.; Zhang, Q.; Li, J.; Cao, G. Mesoporous Vanadium Pentoxide Nanofibers with Significantly Enhanced Li-Ion Storage Properties by Electrospinning. *Energy Environ. Sci.* **2011**, *4*, 858–861.
15. Yan, J.; Sumboja, A.; Khoo, E.; Lee, P. S. V_2O_5 Loaded on SnO_2 Nanowires for High-Rate Li Ion Batteries. *Adv. Mater.* **2011**, *23*, 746–750.
16. Liu, J.; Xia, H.; Xue, D.; Lu, L. Double-shelled Nanocapsules of V_2O_5-based Composites as High-Performance Anode and Cathode Materials for Li Ion Batteries. *J. Am. Chem. Soc.* **2009**, *131*, 12086–12087.
17. Chen, Z.; Qin, Y.; Weng, D.; Xiao, Q.; Peng, Y.; Wang, X.; Li, H.; Wei, F.; Lu, Y. Design and Synthesis of Hierarchical Nanowire Composites for Electrochemical Energy Storage. *Adv. Funct. Mater.* **2009**, *19*, 3420–3426.
18. Seng, K. H.; Liu, J.; Guo, Z. P.; Chen, Z. X.; Jia, D.; Liu, H. K. Free-Standing V_2O_5 Electrode for Flexible Lithium Ion Batteries. *Electrochem. Commun.* **2011**, *13*, 383–386.
19. Sakamoto, J. S.; Dunn, B. Vanadium Oxide-Carbon Nanotube Composite Electrodes for Use in Secondary Lithium Batteries. *J. Electrochem. Soc.* **2002**, *149*, A26–30.
20. Sathiya, M.; Prakash, A. S.; Ramesha, K.; Tarascon, J. M.; Shukla, A. K. V_2O_5-Anchored Carbon Nanotubes for Enhanced Electrochemical Energy Storage. *J. Am. Chem. Soc.* **2011**, *133*, 16291–16299.
21. Gui, X.; Cao, A.; Wei, J.; Li, H.; Jia, Y; Li, Z.; Fan, L.; Wang, K.; Zhu, H.; Wu, D. Soft, Highly Conductive Nanotube Sponges and Composites with Controlled Compressibility. *ACS Nano* **2010**, *4*, 2320–2326.
22. Hu, L.; Wu, H.; Gao, Y.; Cao, A.; Li, H.; McDough, J.; Xie, X.; Zhou, M.; Cui, Y. Silicon-Carbon Nanotube Coaxial Sponge as Li-Ion Anodes with High Areal Capacity. *Adv. Energy Mater.* **2011**, *1*, 523–527.
23. George, S. M. Atomic Layer Deposition: An Overview. *Chem. Rev.* **2010**, *110*, 111–131.
24. Peng, Q.; Lewis, J. S.; Hoertz, P. G.; Glass, J. T.; Parsons, G. N. Atomic Layer Deposition for Electrochemical Energy Generation and Storage Systems. *J. Vac. Sci. Technol. A* **2012**, *30*, 010803.
25. Knoops, H. C. M.; Donders, M. E.; van de Sanden, M. C. M.; Notten, P. H. L.; Kessels, W. M. M. Atomic Layer Deposition for Nanostructured Li-Ion Batteries. *J. Vac. Sci. Technol. A* **2012**, *30*, 010801.
26. Marichy, C.; Bechelany, M.; Pinna, N. Atomic Layer Deposition of Nanostructured Materials for Energy and Environmental Applications. *Adv. Mater.* **2012**, *24*, 1017–1032.
27. Das, R. K.; Liu, B; Reybolds, J. R.; Rinzler, A. G. Engineered Macroporosity in Single-Wall Carbon Nanotube Films. *Nano Lett.* **2009**, *9*, 677–683.
28. Zadin, V.; Brandell, D.; Kasemägi, H.; Aabloo, A.; Thomas, J. O. Finite Element Modelling of Ion Transport in the Electrolyte of a 3D-Microbattery. *Solid State Ionics* **2011**, *192*, 279–283.
29. Meng, X.; Ionescu, M.; Banis, M. N.; Zhong, Y.; Liu, H.; Zhang, Y.; Sun, S.; Li, R.; Sun, X. Heterostructural Coaxial Nanotubes of CNT@Fe_2O_3 *via* Atomic Layer Deposition: Effects of Surface Functionalization and Nitrogen-doping. *J. Nanopart. Res.* **2010**, *13*, 1207–1218.
30. Farmer, D. B.; Gordon, R. G. Atomic Layer Deposition on Suspended Single-Walled Carbon Naotubes *via* Gas-Phase Noncovalent Functionalization. *Nano Lett.* **2006**, *6*, 699–703.
31. Chen, X.; Pomerantseva, E.; Banerjee, P.; Gregorczyk, K.; Ghodssi, R.; Rubloff, G. Ozone-Based Atomic Layer Deposition

of Crystalline V_2O_5 Films for High Performance Electrochemical Energy Storage. *Chem. Mater.* **2012**, *24*, 1255–1261.
32. Perez, I.; Robertson, E.; Banerjee, P.; Henn-Lecordier, L.; Son, S. J.; Lee, S. B.; Rubloff, G. W. TEM-Based Metrology for HfO_2 Layers and Nanotubes Formed in Anodic Aluminum Oxide Nanopore Structures. *Small* **2008**, *4*, 1223–1232.
33. Banerjee, P.; Chen, X.; Gregorczyk, K.; Henn-Lecordier, L.; Rubloff, G. W. Mixed Mode, Ionic-Electronic Diode Using Atomic Layer Deposition of V_2O_5 and ZnO Films. *J. Mater. Chem.* **2011**, *21*, 15391–15397.
34. Elam, J. W.; Routkevitch, D.; Mardilovich, P. P.; George, S. M. Conformal Coating on Ultrahigh-Aspect-Ratio Nanopores of Anodic Alumina by Atomic Layer Deposition. *Chem. Mater.* **2003**, *15*, 3507–3517.
35. Zhang, Z.; Dewan, C.; Kothari, S.; Mitra, S.; Teeters, D. Carbon Nanotube Synthesis, Characteristics, and Microbattery Applications. *Mater. Sci. Eng., B* **2005**, *116*, 363–368.
36. Golodnitsky, D.; Nathan, M.; Yufit, V.; Strauss, E.; Freedman, K.; Burstein, L.; Gladkich, A.; Peled, E. Progress in Three-Dimensional (3D) Li-Ion Microbatteries. *Solid State Ionics* **2006**, *177*, 2811–2819.
37. Le Van, K.; Groult, H.; Mantoux, A.; Perrigaud, L.; Lantelme, F.; Lindström, R.; Badour-Hadjean, R.; Zanna, S.; Lincot, D. Amorphous Vanadium Oxide Films Synthesised by ALCVD for Lithium Rechargeable Batteries. *J. Power Sources* **2006**, *160*, 592–601.
38. Nagasubramanian, G.; Doughty, D. H. Electrical Characterization of All-Solid-State Thin Film Batteries. *J. Power Sources* **2004**, *136*, 395–400.
39. Cheah, S. K.; Perre, E.; Rooth, M.; Fondell, M.; Harsta, A.; Nyholm, L.; Boman, M.; Gustafsson, T.; Lu, J.; Simon, P.; Edstrom, K. Self-Supported Three-Dimensional Nanoelectrodes for Microbattery Applications. *Nano Lett.* **2009**, *9*, 3230–3233.
40. Pomerantseva, E.; Gerasopoulos, K.; Chen, X.; Rubloff, G. W.; Ghodssi, R. Electrochemical Performance of the Nanostructured Biotemplated V_2O_5 Cathode for Lithium-Ion Batteries. *J. Power Sources* **2012**, *206*, 282–287.
41. Zhu, Q.; Chen, N.; Tao, F.; Pan, Q. Improving the Lithium Storage Properties of Fe_2O_3@C Nanoparticles by Superoleophilic and Superhydrophobic Polysiloxane Coatings. *J. Mater. Chem.* **2012**, *22*, 15894–15900.